

Vibration characterization and mitigation for the Gemini MCAO system GeMS

Ignacio Rodriguez¹, Benoit Neichel², Markus Hartung², Thomas Hayward², Julian Christou³, Francois Rigaut², Dani Guzman¹, James Osborn¹, Andres Guesalaga^{1*}

¹ Universidad Católica de Chile, 4860 Vicuna Mackenna, Casilla 7820436, Santiago, Chile

² Gemini Observatory Southern Operations Center, Casilla 603, La Serena, Chile

³ Gemini Observatory Northern Operations Center, 670 N.A^oOhoku Place, Hilo HI96720, USA

*corresponding author: aguesala@ing.puc.cl

Abstract. We describe the methods used to mitigate the vibrations encountered in some of the instruments of the Gemini South telescope. We found a persistent vibration at 55Hz with others occurring occasionally at 14 and 100Hz. Two types of AO controllers -Kalman and H_∞ - were implemented in the MCAO Tip-Tilt loop. First results show clear improvements in vibration rejection and overall performance for these advanced controllers over the classical integrator. It is shown that the reduction in the standard deviation of residual slopes is highly dependent on turbulence, wind speed and vibration conditions, ranging -in slopes RMS- from an almost negligible reduction for high speed wind to a factor of 5 for a combination of low wind and strong vibrations.

1. Introduction

As AO systems become better at correcting the atmospheric turbulence, other factors such as vibrations in the instruments and the telescope become increasingly important to gain the next step in performance [1-3]. As an AO system can correct for the turbulence, it can also be used to compensate other sources of perturbations. This concept have been already tested at laboratory level [4] and recently started to be used on operational systems [5]. They are considered essential for the future Extremely Large Telescopes [5,6].

In this paper we describe the characterization of the vibrations and testing of different control techniques on a Multi-Conjugate Adaptive Optics (MCAO) system: the Gemini MCAO System (GeMS), installed at the Gemini South Observatory. The vibrations are characterized by a spectral analysis of the GeMS WFS and Gemini South Adaptive Optics Imager (GSAOI) images. We then use this data to artificially induce similar vibrations with a tip/tilt mirror and simulate atmospheric turbulence on the GeMS optical bench. This allows us to run several control algorithms in a controlled environment, and test them in a few different scenarios. Three control laws have been implemented: the classic integrator, Linear Quadratic Gaussian (LQG) (based on a Kalman estimator) [7,8] and H_2/H_∞ [9,10] synthesis methods.

2. Vibration characterization for GeMS

GeMS uses 5 artificial Laser Guide Stars (LGS) with their associated LGS wavefront sensors (LGSWFS) and 3 Deformable Mirrors (DM) to compensate the turbulence over a Field of View of 2 arcmin. Besides this, 3 Natural Guide Stars (NGS) are required for the control of the

Adaptive Optics for Extremely Large Telescopes II

Tip-Tilt and plate scale modes. The NGS consists of 3 probes, each containing a reflective pyramid that acts like a quad-cell feeding a set of 4 fibers+APDs. Three NGS wavefront sensors (NGSWFS) provide six X-Y slopes necessary to generate global tip and tilt residuals that feed a Tip-Tilt Mirror (TTM) controller residing in the Real Time Controller (RTC). Plate scale modes can also be estimated from this set of slopes [11] but they are not considered in this paper. The Laser loop and the NGS loop can be driven at a rate of up to 800Hz.

GeMS delivers a uniform, diffraction-limited corrected near-infrared (NIR) image to GSAOI which can provide a fast reading of On-Detector Guide Window (ODGW), also at a rate of up to 800Hz. These ODGW can be used to control the TTM, or to monitor the performance at the science detector level. The optical bench also includes calibration sources that can generate artificial stars (either Laser or Natural guide stars) and that has been extensively used in this work. The DM and the TTM can be used to generate perturbations to simulate turbulence or vibrations. More details about GeMS can be found in [12].

Plots in figure 1-left show the power spectra acquired with the NGSWFS. The main feature that appears on these PSDs is a strong vibration peak around 55Hz for the Y-axis. We have identified that the cryo-coolers of GSAOI were producing this vibration. In figure 1-right, we show the power spectral density (PSD) of the Y-axis as measured by the LGSWFS, and the spot motion on the ODGW (coarse line). These plots are in a PSD \times frequency representation, in order to emphasize the distribution of the energy among the different contributors.

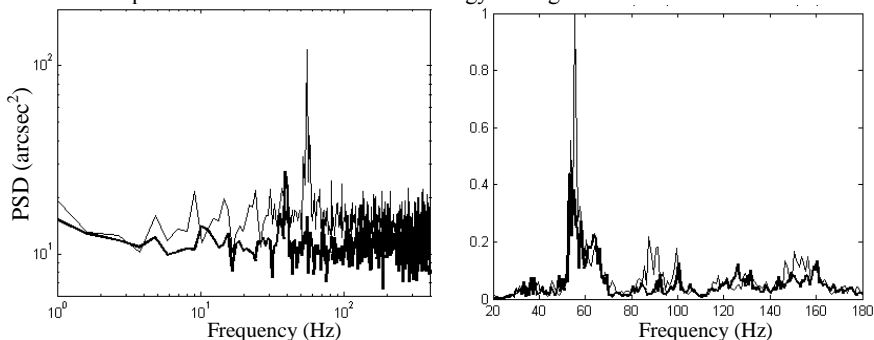


Figure 1. Data from calibration sources. Left panel: PSDs for NGSWFS (Tip or X is coarse line and Tilt/Y is fine line). Right panel: LGSWFS (fine) and GSAOI-ODGW (coarse). The plots on the right panel are in a PSD \times frequency representation to emphasize the distribution of energy

An example of PSD measured on-sky at the LGSWFS level is presented in figure 2 (left) for the Tilt direction. The 55 Hz peak is clearly detected, which confirms that this vibration lies in the common optical path. Some higher frequency sharp peaks are also seen, some of them not being detected by the NGSWFS, due to noise, or non-common path effect.

In order to compare different control algorithms, we have generated typical vibrations and seeing conditions on the bench, by artificially exciting the TTM. Based on the on-sky data, we have chosen three vibrations peaks: 14Hz, 55Hz, and 100Hz. In addition, we chose to simulate two seeing conditions: a slow turbulence with a cut-off frequency around 15Hz, and a fast turbulence with a cut-off frequency around 100Hz. These cases will allow us to compare the behavior of the different control algorithm for representative conditions seen by GeMS.

Adaptive Optics for Extremely Large Telescopes II

Figure 2 (right) shows three examples of OL data simulated on the bench, as measured by the LGSWFS that we will use later in this paper. The plots are: (i) a slow seeing and 55Hz vibration (continuous line), (ii) a slow seeing and 14Hz vibration (dashed line) and (iii) a fast seeing and a 100Hz vibration (dotted line, right panel).

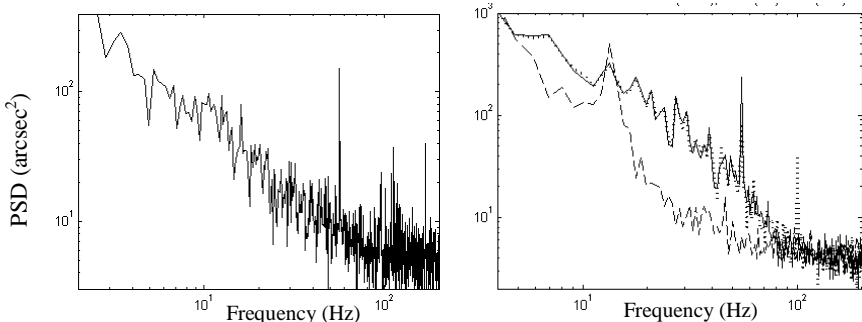


Figure 2. Left panel: On-sky PSDs for the LGSWFS. Data acquire in March 2011. Right panel: slow seeing and 55Hz vibration (continuous line); slow seeing and 14Hz vibration (dashed line); fast seeing and a 100Hz vibration (dotted line)

3. Controller theory

In this section, three controllers are designed for a later implementation in GeMS.

3.A. Integrator

The current default tip-tilt controller in CANOPUS is the classical integrator:

$$C(z) = \frac{K_i}{1 - az^{-1}} \quad (1)$$

where z is the Z-transform operator and a is generally unity, unless a “leaky” integrator is desired. Parameter K_i represents the gain of the loop and is adjusted according to noise and performance requirements. An optimal way to define this gain is proposed by Gendron [13].

3.B. Kalman

The Kalman approach (or LQG) provides an optimal correction criterion for the mirror commands (voltages) that minimize the variance of the slope residuals. The problem is split into a stochastic estimation problem and a deterministic control problem. The first step estimates the turbulence phase by minimizing a stochastic criterion (Kalman filter); the second finds the best commands for the TTM, assuming negligible dynamics, i.e. a static projection of the estimated state-space values onto the TTM modes [7]. For more information on this method the reader is referred to [4,7,14].

3.C. H_∞ control

Looking for new contributions to this challenging control problem, we suggest the use of frequency-based design techniques. These syntheses techniques based on the minimization of H_2 and H_∞ norms [9,10], seem particularly suitable to tackle vibration rejection problems, and can readily take TTM loop dynamics and performance requirements the design stages.

Adaptive Optics for Extremely Large Telescopes II

In this frequency approach the controller $G(z)$ is synthesized to reduce the mixed-sensitivity norm [10]. This norm is formed as a weighted combination of the Sensitivity Function (SF), the Control Sensitivity Function (CSF) associated to control energy usage and the Noise Transfer Function (NTF). Contrary to the Kalman approach, we use the CSF instead of the NTF because this function not only can be used to restrict the use of actuator signal, but also to avoid excessive noise amplification by weighing the CSF at higher frequencies.

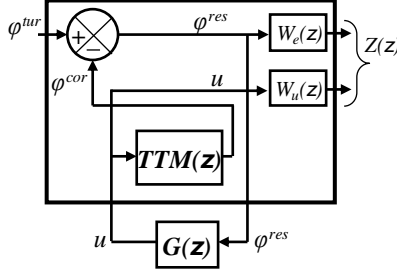


Figure 3. The augmented representation used to synthesize the H^∞ controller, $G(z)$.

Figure 3 shows the so-called augmented representation, where the weighting functions are the distinctive characteristic. Function $W_e(z)$ penalize control errors and $W_u(z)$ weighs the actuator signal, so it restricts its usage at some frequencies. The latter can be used to attenuate the effect of noise amplification in the loop, i.e. a controller with a low-pass characteristic. These two weighting functions are normally complementary, so that the contradictory requirements that good accuracy and control effort impose on the design, can be met by the resulting controller. The reader will find a comprehensive tutorial in reference [9].

Doyle *et al.* [9] demonstrate that the computation for H_2 and the H^∞ solutions requires solving two Riccati equations in their static form (optimal estimation and optimal control problems). The H^∞ norm corresponds to the highest value (worst case) of the spectrum to be minimized, so it can be more appropriate in cases where resonances exist.

The controller $G(z)$ is derived from the minimization of the H^∞ norm [10] given by:

$$\min_G \|Z\|_\infty = \min_G \left\| \begin{array}{c} W_e \cdot SF \\ W_u \cdot CSF \end{array} \right\|_\infty \quad (2)$$

In the previous Kalman approach, the disturbances are modeled to account for turbulence and vibration spectral amplitude. Here, they are assumed to have a flat spectrum and the information on the turbulence and vibration strength is contained in the $W_e(z)$ function used during the controller synthesis so that each frequency is weighed according to its intensity. The physical limitations of the actuators (dynamic and static) are represented by function $W_u(z)$.

4. A design example for tip-tilt control the H^∞ method

Open-loop tip-tilt slopes were collected from NGSWFSSs, showing a strong peak at 55 Hz (figure 4). In order to tackle both the turbulence and the vibration, W_e is fitted to the standard deviation of slopes using rational functions (equation (3)). Function W_e weighs the error signal at low frequencies and also at a specific vibration frequency.

Adaptive Optics for Extremely Large Telescopes II

$$W_e(s) = \frac{C_0}{s + C_1} \cdot \frac{s^2 + 2\eta_1\omega_o s + \omega_o^2}{s^2 + 2\eta_2\omega_o s + \omega_o^2}, \quad C_1 \ll C_0 \quad (3)$$

where C_0 and C_1 are determined by the turbulence and ω_o corresponds to the vibration frequency. The damping factors η_1 and η_2 define the height and width of the peak.

The mirror dynamics represented by $TTM(z)$, was experimentally found to be:

$$TTM(s) = \frac{1}{0.0025s + 1} \quad (4)$$

In the H_∞ approach the TTM bandwidth is included by shaping function W_u with a high-pass characteristic that penalizes the use of control signals above the cutoff frequency and also reduces the sensitivity of the controller to high frequency noise. Mathematically:

$$W_u(s) = C_2 \cdot \frac{s}{C_3 s + 1} \quad (5)$$

where C_2 and C_3 are adjusted to represent the characteristic of the TTM bandwidth and noise.

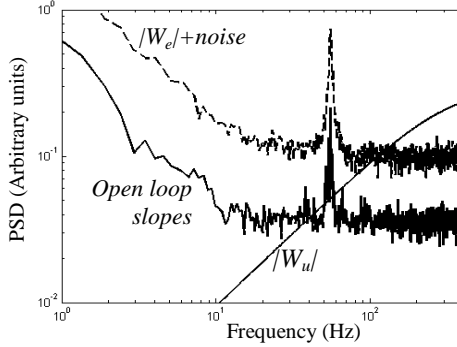


Figure 4. Fitting of W_e to OL NGS-WFS data and W_u (W_e plot has been vertically displaced for clarity). Data taken from observations on February 11th, 2011

Figure 4 shows the result of fitting function W_e and noise to the data (the fitting is vertically displaced for clarity).

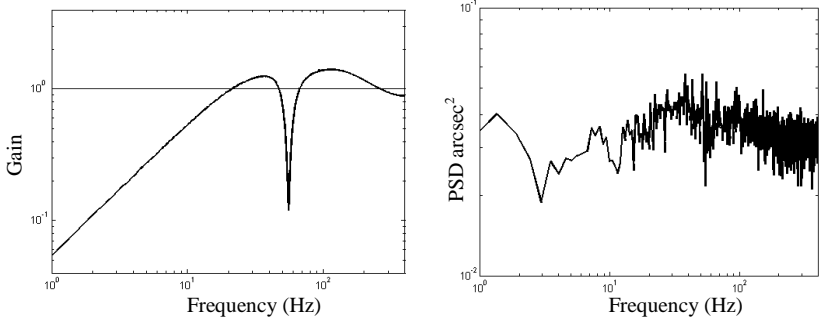


Figure 5. SF obtained by H_∞ synthesis (left) and PSD of residuals with the H_∞ controller (right).

Adaptive Optics for Extremely Large Telescopes II

A fifth order controller is obtained after the synthesis process described above, with figure 5 (left) showing the SF of the resulting closed-loop system. As previously reported [15], the squared sensitivity function is approximately proportional to the inverse of the disturbance in figure 4. Figure 5 (right) shows a plot of the PSD of the residuals obtained for the closed-loop system. As expected, the close-loop residual response tends to be flat for both advanced controllers. In the next section, the RMS value of these residuals will be used to compare the performances of the three different controllers.

5. Results

In this section we compare the performance of the controllers when the input conditions are changing. The Kalman and H^∞ controllers described above have been implemented in the RTC, for notches at 14Hz, 55Hz and 100Hz. In figure 6 (left) we show the SF for the first case. For a fair comparison among controllers, they were finely tuned to get similar overshoots in the SF function (around 8dB). We show a restricted frequency domain for a better visualization.

The controllers' performance was tested for three different types of turbulences: Case I: Wind speed matched to $1/SF$ and medium strength vibrations; Case II: Slow wind and strong vibrations; and Case III: Fast wind and weak vibrations. Vibrations were induced artificially in the loop by exciting the TTM. GSAOI was not available for this experiment so the techniques were evaluated using the standard deviation of slopes at the NGSWFS and LGSWFS. We use the LGSWFSs as a scoring camera to assess the three controllers, as the PSDs observed at the GSAOI and LGSWFSs were highly correlated. The following analysis is carried out only for the Tilt loop, since it is the direction where most of the disturbance appeared.

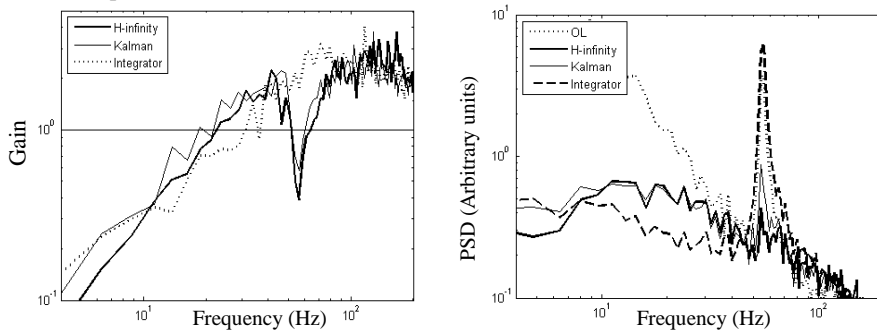


Figure 6. Left panel: SF for the three controllers in the case of a notch at 55 Hz. Right panel: Case I, 55 Hz: SF for OL Integrator, Kalman and H^∞ controllers

5.A. Case I: Wind speed matched to $1/SF$ and medium strength vibrations

This case analyses the performance of the closed-loop system when the actual turbulence matches the disturbance model assumed during the design of Kalman and H^∞ controllers (i.e. $1/SF$). Figure 6 (right) shows the PSD for open loop, integrator, Kalman and H^∞ for a vibration frequency of 55 Hz.

The Kalman and H^∞ controllers reject the disturbance effectively, and close loop residuals are flat. For the 14Hz vibration (not shown), the integrator can reduce partially the vibration, but

Adaptive Optics for Extremely Large Telescopes II

for the 55Hz, it makes the situation worse due to an SF gain higher than 1 at such frequencies. This is where the advanced controller can provide most of the benefit.

For these specific cases, improvement in performance brought by Kalman and H_∞ are of the order of 20%. Due to Bode's theorem [16], the advanced controllers provide better rejection on the vibrations, but at the expense of a worse performance at medium and low frequencies, i.e. the attenuation of SF in one frequency band is compensated by a loss in another frequency range. This tell us that the advantage of the advanced controllers is that they reject disturbance effects where their effect is stronger.

In summary, for a case where the filter matches the perturbation, significant improvements in performance can be achieved by advanced controller compare to the classical integrator.

5.B. Case II: Slow wind and strong vibrations

We now modify the inputs for a slower turbulence and higher amplitude vibrations, where Kalman and H_∞ controllers are particularly well suited, since the turbulence spectrum is far from the loop bandwidth. Any improvement in vibrations rejection will have a much higher impact on the overall performance, i.e. advanced controllers will outperform the integrator by a large factor. This is confirmed in table 1, where the residuals generated by Kalman and H_∞ controllers are reduced by a factor of 3 to 5 when compared to those of the integrator.

5.C. Case III: Fast wind and weak vibrations

In this case, we introduce a faster turbulence, reducing the amplitude of the vibrations. This is the worst possible condition for the advanced controllers, i.e. fast turbulence with components similar or higher than the loop cutoff frequency. The higher SF gains at central frequencies erase any possible improvement obtained by rejecting these vibrations.

Table 1. RMS of residual slopes (normalized to the integrator residual variance). LGS data and 100Hz vibration data only show for case I.

Controller	14 Hz				55 Hz				100 Hz	
	I		II	III	I		II	III	I	
	NGS	LGS			NGS	LGS			NGS	LGS
Open-loop	5.25	5.63	22.63	2.39	5.29	5.83	3.89	2.32	6.69	6.82
Integrator	1.0	1.0	1.0	1.0	1.0	1.0	1.0	1.0	1.0	1.0
Kalman	0.88	0.88	0.63	0.9	0.83	0.83	0.31	1.0	0.94	0.88
H_∞	0.88	0.88	0.63	1.0	0.78	0.83	0.23	0.97	0.94	0.88

6. Results

Results presented above show significant gains for Kalman and H_∞ controllers over a standard integrator, when turbulence is weak or when the disturbance is proportional to the inverse of the controllers' SF. For faster turbulence (higher wind speeds) this advantage vanishes, mainly due to the closed-loop bandwidth.

The results obtained in cases II and III demonstrate that matching the vibration and turbulence accurately is essential for a good performance of the Kalman and H_∞ controllers. By correctly identifying the turbulence frequency spectrum better rejection of vibrations can be expected. The latter suggests the need for more sophisticated on-line identification techniques to provide the best rejection possible as the characteristics of the turbulence and disturbances change.

The main benefit in using sophisticated controllers is that the SF is shaped to tackle specific frequencies where disturbances are concentrated reducing the controller impact in other parts of the spectrum. Although the theory behind Kalman and H_∞ controllers ensure a flat

Adaptive Optics for Extremely Large Telescopes II

spectrum of residuals in this optimal case, the actual results tend to miss expectations. This is mainly due to inaccurate modeling of disturbances, non-linearities or dynamics present in the loop and not modeled (e.g. mirror dynamics). This suggests that relying on identification tools for finding the turbulence and vibration parameters to tune the controllers might not be the right choice. We think that an on-line tuning of the controllers looking for the lowest and balanced PSD of the measured residuals should be investigated.

Due to Bode's theorem, the two advanced controllers can always be shaped to generate similar performances, and both approaches reject the vibration frequency effectively, so the overall residual indices improve significantly when compared to the classical integrator.

Acknowledgments

We thank to the Chilean Research Council, grants Fondecyt 1095153 and Anillo ACT-86.

References

1. J. Maly, E. Darren and T. Pargett, Vibration Suppression for the Gemini Planet Image, Proceedings of the SPIE, vol. 7733, 7731F (2010).
2. Y. Clenet, M. Kasper, N. Ageorges, C. Lidman, T. Fusco, G. Rousset, O. Marco, M. Hartung, D. Mouillet, B. Koehler, and N. Hubin, NACO performance: Status after 2 years of operation, Proceedings of the SPIE, vol. 5490 (2004).
3. J. P. Verán and L. Poyneer L., Evaluation of the T/T Conditions at Gemini South Using NICI AO Telemetry Data, 1st AO4ELT Conference, Paris, June 22-26, 2009.
4. C. Petit, J. M. Conan, T. Fusco, J. Montri, C. Kulcsár, H. F. Raynaud and D. Rabaud, First laboratory demonstration of closed-loop Kalman based optimal control for vibration filtering and simplified MCAO, Proceedings SPIE, vol. 6272 (2006).
5. G. Agapito, F. Quirós-Pacheco, P. Tesi, A. Riccardi, and S. Esposito, Observer-Based Control Techniques for the LBT Adaptive Optics under Telescope Vibrations, European Journal of Control, vol 17(3), pp. 316 – 326 (2011).
6. J. M. Conan, H. F. Raynaud, C. Kulcsár, S.Meimon, Are integral controllers adapted to the new era of ELT adaptive optics?, 2nd AO4ELT, Victoria, Canada, 25-30 Sept., 2011.
7. B. LeRoux, J.M. Conan, C. Kulcsár, H.F. Raynaud, L.M. Mugnier and T.Fusco, Optimal Control Law for Classical and Multiconjugate Adaptive Optics, J.Opt.Soc.Am. A, vol. 21, pp.1261-1276 (2004).
8. C. Kulcsár, H.-F. Raynaud, C. Petit, J.-M. Conan, et P. Viaris de Lesegno. Optimal control, observers and integrators in adaptive optics. Opt.Express, 14, pp.7464-7476, 2006.
9. J. C. Doyle, K. Glover, P.P. Khargonekar, and B. A. Francis, State-space solutions to standard H₂ and H_∞ control problems, IEEE Transactions on Automatic Control vol. 34, pp.831-847 (1989).
10. M. G. Safonov, D. J. N. Limebeer and R. Y. Chiang, Simplifying the H_∞ theory via loop shifting, matrix pencil and descriptor concepts, Int. J. Contr., vol. 50, pp.2467-88 (1989).
11. B. L. Ellerbroek and F. Rigaut., Methods for correcting tilt anisoplanatism in laser-guide-star-based multiconjugate adaptive optics, J. Opt. Soc. Am. A, 18, 2539-2547 (2001).
12. F. Rigaut., Neichel B., Gemini South MCAO on-sky results, 2nd AO4ELT Conference, Victoria, Canada, 25-30 Sept., 2011.
13. E. Gendron and P. Lena, Astronomical adaptive optics I. modal control optimization, Astron. Astrophys. 291, pp337 (1994).
14. C. Correia, H. F. Raynaud, C. Kulcsár and J. M. Conan, On the optimal reconstruction and control of adaptive optical systems with mirror dynamics, J. Opt. Soc. Am. A, Vol. 27(2), pp. 333-349 (2010).
15. S.Meimon, C.Petit, T.Fusco, and C.Kulcsár, Tip-tilt disturbance model identification for Kalman-based control scheme: application to XAO and ELT systems, JOSAA, vol 27,pp.122-132 (2010).
16. C. Mohtadi, Bode's integral theorem for discrete-time systems, Control Theory and Applications, IEE Proceedings Part D, vol. 137, pp57-66 (1990).